Importance of the upper-level warm core in the rapid intensification of a tropical cyclone

Da-Lin Zhang[1] and Hua Chen[1]

Received 6 December 2011; revised 25 December 2011; accepted 27 December 2011; published 28 January 2012.

[1] In this study, the rapid intensification (RI) of tropical cyclone is examined using a 72-h cloud-permitting prediction of Hurricane Wilma (2005) with a record-breaking intensity of 882 hPa. Results show the formation of an upper-level warm core from the descending air of stratospheric origin in the eye, which coincides with the onset of RI; it reaches the peak amplitude of more than 18°C from its initial conditions at the time of peak intensity. The descending air is associated with the detrainment of convective bursts in the eyewall, and it appears as (perturbation) cyclonic radial inflows above the upper outflow layer and causes the subsidence warming below. We hypothesize that the upper divergent outflow layer favors the generation of a warm core by protecting it from ventilation by environmental flows. Use of the hydrostatic equation shows that the warm core of stratospheric origin contributes more than twice as much as the lower-level warm column to the pressure change at the peak intensity of Wilma. Results suggest that more attention be paid to the magnitude of storm-relative flows and vertical wind shear in the upper troposphere, rather than just vertical shear in the typical 850–200 hPa layer, in order to reasonably predict the RI of tropical cyclones. **Citation:** Zhang, D.-L., and H. Chen (2012), Importance of the upper-level warm core in the rapid intensification of a tropical cyclone, *Geophys. Res. Lett.*, *39*, L02806, doi:10.1029/2011GL050578.

1. Introduction

[2] The rapid intensification (RI) of hurricanes, defined as at least a 42 hPa day^{-1} drop in the minimum central pressure (P_{MIN}) [*Holliday and Thompson*, 1979] or a 15 m s^{-1} day^{-1} increase in the maximum surface wind (V_{MAX}) [*Kaplan and DeMaria*, 2003], is particularly challenging for operational forecasts due partly to deficiencies in hurricane models and partly to the poor understanding of the physical processes leading to the generation of these rare events. Most of our current understanding of RI is limited to environmental conditions that can be examined from large-scale analyses and satellite observations [*Bosart et al.*, 2000; *Kaplan and DeMaria*, 2003]. Favorable conditions for RI may include anomalously warm sea surface temperatures (SSTs), high relative humidity in the lower troposphere, weak vertical shear of the horizontal wind (VWS), and weak forcing from upper-level troughs with easterly flows aloft. In addition, *Kaplan and DeMaria* [2003] find that a hurricane that is far from its maximum potential intensity (MPI) has the greatest chance of undergoing RI under the favorable conditions. Hurricane Opal (1995) is a good example of RI that has received much attention [*Rodgers et al.*, 1998; *Bosart et al.*, 2000; *Shay et al.*, 2000; *Hong et al.*, 2000].

[3] More recent studies of RI begin to examine the possible processes taking place in the inner-core regions of hurricanes [*Kaplan et al.*, 2010; *Rogers*, 2010]. Convective bursts (CBs), loosely defined by previous researchers to imply anomalous intense updrafts in a mesoscale convective system, have been considered as a powerful candidate for RI. Many observational studies show that CBs either preceded RI or coincided with the onset of RI [e.g., *Molinari et al.*, 1994, 1999; *Reasor et al.*, 2009; *Heymsfield et al.*, 2001; *Fierro and Reisner*, 2011]. However, little is known about the roles of CBs in causing RI. Upward transport of enthalpy-rich air by supergradient outflows in the eye boundary layer, as first shown by *Liu et al.* [1999], has been hypothesized as being favorable for the development of CBs [*Kossin and Eastin*, 2001; *Eastin et al.*, 2005; *Braun et al.*, 2006; *Braun and Wu*, 2007; *Barnes and Fuentes*, 2010]. *Montgomery et al.* [2006] argue that this transport can result in a hurricane exceeding its MPI. In addition, by analyzing 6 hourly lightning data during the life cycle of 56 hurricanes, *Price et al.* [2009] find that increased lightning activity preceded the maximum intensities for all of these hurricanes, approximately one day prior to the occurrence of peak surface winds.

[4] In this study, we hypothesize that the formation of an intense warm core within the upper outflow layer, resulting from the detrainment of CBs from the eyewall, is the key to the RI of hurricanes. This hypothesis will be examined using a successful 72-h (i.e., 0000 UTC 18 – 0000 UTC 21 October 2005) nested-grid (27/9/3/1 km), cloud-permitting prediction of Hurricane Wilma with the Weather Research Forecast (WRF) model at the finest grid length of 1 km (see *Chen et al.* [2011] for more details). The 72-h period covers an initial 15-h spin up, a 21-h RI and a 36-h weakening stage (Figure 1, bottom). *Chen et al.* [2011] show that Wilma's RI occurred in the presence of high SSTs and weak VWS, and that the WRF model predicts about a 28 m s^{-1} increase in V_{MAX} and an 80 hPa drop in P_{MIN} during the 21-h RI period, with P_{MIN} = 889 hPa and V_{MAX} = 72 m s^{-1}. The next section shows the importance of an upper-level warm core in determining the RI of Wilma in terms of drops in P_{MIN}, and section 3 explores how this upper-level warm core is generated.

2. Importance of the Upper-Level Warm Core in RI

[5] Figure 1 shows the time-height cross section of perturbation temperatures [$T'(z, t)$] in relation to the time series of P_{MIN} drops (P') with respect to the mean vertical

[1]Department of Atmospheric and Oceanic Science and Center for Scientific Computation and Mathematical Modeling, University of Maryland, College Park, Maryland, USA.

0094-8276/12/2011GL050578

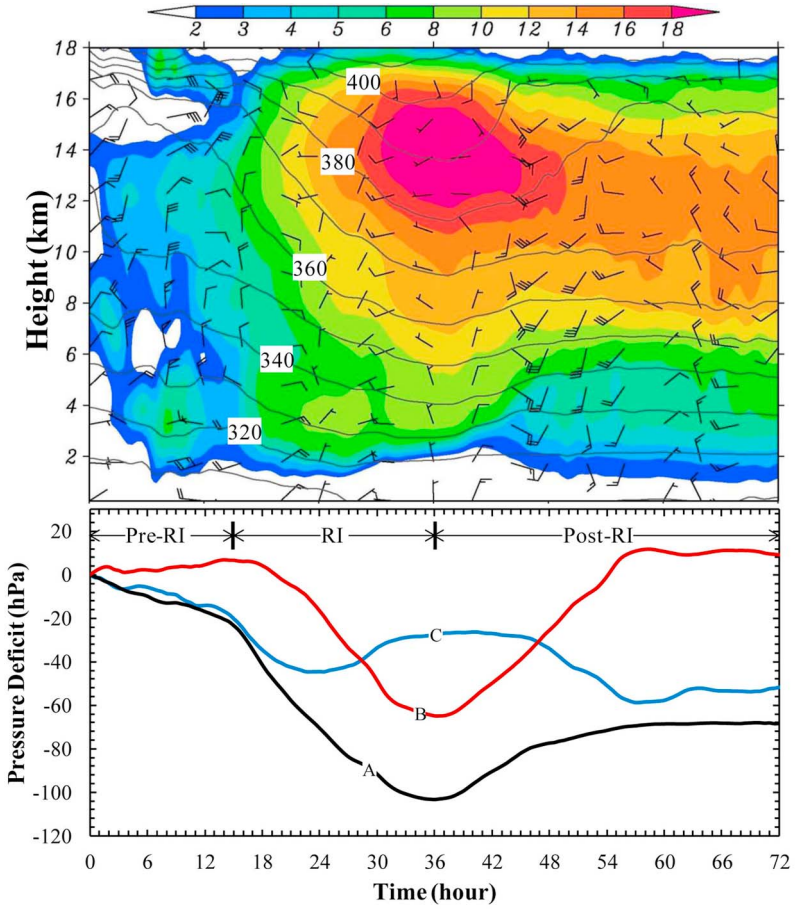

Figure 1. (top) Time-height cross section of temperature changes (T', shaded), superposed with potential temperature (θ, contoured at intervals of 10 K) and storm-relative flows (a full barb is 5 m s^{-1}), at the eye center from the 72-h prediction of Hurricane Wilma (2005) at the 3-km resolution and 30-min intervals, where T' are defined with respect to the (1000 km × 1000 km) area-averaged temperatures at the model initial time ($\bar{T}$). (bottom) Time series of P_{MIN} drops (P') reproduced from the 72-h prediction (curve A), P' estimated from the warm column above the θ = 380-K surface (curve B), and from the warm column beneath the θ = 380-K surface (curve C), where P′ is defined with respect to P_{MIN} at the model initial time.

temperature profile [$\bar{T}(z)$] and P_{MIN} at the model initial time (i.e., t = 0), respectively, superimposed with storm-relative flows, at the eye center. We see that the hurricane vortex initially has a warm core of 4–5°C centered near z = 7 km. After the initial 6–12 h spin-up, a shallow upper warming layer of 6–8°C appears above a deep warming column in the eye. For the sake of convenience in relating the results shown in Figures 1 (top) and 1 (bottom), we use the word "warming" to imply a positive temperature change(s) with respect to $\bar{T}(z)$ at t = 0 in the storm-relative framework, although the environmental temperature changes during the 72-h prediction are small. Of importance is that this warming occurs in the stratosphere, as indicated by larger vertical potential temperature (θ) gradient above z = 16 km. Since the model top is set at 30 hPa [see *Chen et al.*, 2011], with a mean altitude of about z = 24 km, this warming is little affected by the top boundary conditions. Of further importance is that the isentropic surfaces in the upper warming layer (e.g., θ = 370–400 K) begin to displace downward at the onset of RI (cf. Figures 1, top and 1, bottom). Because little diabatic heating occurs near the eye center, this downward displacement indicates subsidence warming associated with the descent of lower stratospheric air in the eye [see *Liu et al.*, 1999]. All the isentropic surfaces in the vertical column descend to their lowest altitudes with the peak warm core occurring at the time of the peak storm intensity (i.e., t = 36 h). During this 21-h RI, the air at the tropopause, as indicated by θ = 370 K, descends from z = 16 to 9 km, leading to a strong warming column of stratospheric origin with the peak amplitude of more than 18°C near z = 14 km. This peak warming core is similar in magnitude to but about 2 km higher than that found in early observational studies of *LaSeur and Hawkins* [1963], *Hawkins and Rubsam* [1968], and *Hawkins and Imbembo* [1976]. Subsequently, the isentropic surfaces tilt upward while the warming core shifts downward and weakens in magnitude during the 36–45 h period when Wilma fills; all these features occur more rapidly than those occurring afterwards.

[6] Since RI is examined herein in terms of surface pressure falls (i.e., P'), we wish to show, through the simple use of the hydrostatic equation, that it is the warming core of stratospheric origin that causes RI of Wilma. Of particular relevance is that under hydrostatic balance warming at lower temperatures aloft can produce much greater impact on

surface pressure falls than lower-level warming because of the more exponential effects of the upper-level warming [*Malkus and Riehl*, 1960; *Zhang and Fritsch*, 1988; *Hirschberg and Fritsch*, 1993; *Holland*, 1997]. In addition, the subsidence warming of stratospheric air tends to be greater in magnitude than that of tropospheric air, as shown in Figure 1 (top). Thus, the upper-level warming, especially with stratospheric origin, is more effective than the lower-level warming in reducing P_{MIN}. Figure 1 (bottom), in which the θ = 380-K surface is used to separate contributions of the warming from stratospheric and tropospheric origins to the time series of P', demonstrates this point. The three curves, labeled as "A", "B", and "C", in Figure 1 (bottom) are obtained as follows: (i) the time series of the model output P_{MIN}, as shown in Figure 4 of *Chen et al.* [2011], is reproduced as P' with respect to P_{MIN} at t = 0 (curve A) by integrating the hydrostatic equation from the model top downward with the total temperatures [i.e., $T = \bar{T}(z) + T'(z, t)$] in order to ensure the absence of significant errors; (ii) repeat step (i) except by setting $T'(z, t) = 0$ in the layers below the θ = 380-K surface (curve B); and (iii) repeat step (i) except by setting $T'(z, t) = 0$ in the layers above the θ = 380-K surface (curve C). Since the θ = 380-K surface originates from the lower stratosphere (Figure 1, top), the results so obtained tend to underestimate contributions of the upper-level warm core.

[7] It is apparent from Figure 1 (bottom) that curve B, representing contributions from the upper-level warming core, resembles in shape curve A including total contributions, and exhibits a 72-hPa fall in P_{MIN} during the 21-h RI, followed by a 76-hPa rise during the 21-h weakening stage. It should be noted that such large variations are also highly dependent on the warm column depth used in the calculations because of the pronounced changes in the elevation of the θ = 380-K surface during and after the RI stage (Figure 1, top). If only the peak intensity at t = 36 h is considered, the warming columns above and below the θ = 380-K surface (located at $z \approx 11$ km) account for a drop in P_{MIN} of 64 hPa (curve B) and 24 hPa (curve C), respectively, from the initial intensity. This indicates that the warming core of stratospheric origin could contribute more than twice as much as the lower-level warming column to pressure changes during the RI of Wilma. Note that the sum of contributions from the warming columns above and below the θ = 380-K surface does not equal the total P_{MIN} deficit because of the exponential dependence of P_{MIN} on temperature changes in the vertical. In the present case, the exponential dependence for the vertical column below the θ = 380-K surface more than doubles the pressure difference obtained between steps (ii) and (iii) at $z \approx 11$ km (i.e., 19 hPa compared to 40 hPa at z = 0). Nevertheless, the warming column below the θ = 380-K surface accounts mostly for the initial spin-up of Wilma (cf. curves C and A). Without the upper-level warming, the storm may cease deepening after 22–24 h into the prediction, and fail to achieve the RI rate.

3. Formation of the Upper-Level Warming Core

[8] After showing the importance of the upper-level warming core, one may ask: Why does it form near z = 14 km in the present case? In particular, we have seen several observational and modeling studies showing the development of midlevel warm core structures [e.g., *Liu et al.*, 1997; *Halverson et al.*, 2006]. To address the above question, Figure 2 shows the radius-height cross section of deviation temperatures, superimposed with in-plane flow vectors, and upper radial inflows during the RI stage (i.e., at t = 30 h). In addition to the typical in- up- and outward secondary circulation of a mature hurricane, two relevant features are worthy of discussion. First, the peak warming core is located in the same (13–15 km) layer as the upper-level outflow in the outer region. We emphasize the importance of this finding because a strong divergent outflow at the scale of 200–400 km in radius could help protect the warming core from being ventilated by environmental flows. Although numerous studies have examined the detrimental impact of VWS in a deep layer on hurricane intensity through the downshear tilt and horizontal ventilation of the core warmth [*Wang and Holland*, 1996; *Frank and Ritchie*, 2001; *Black et al.*, 2002], little attention has been paid to horizontal wind intensity and structures in the upper warm-core and outflow layer. An analysis of the time series of vertical wind profiles in the eye, as given in Figure 1 (top), reveals that changes in the upper-level warming-core intensity are indeed correlated with the magnitudes of storm-relative flows. Specifically, the storm-relative flows in the eye are about 10–20 m s^{-1} in a deep layer (i.e., z = 2–18 km) during the pre-RI stage, although such large flows could be partly attributed to the vertical tilt of the hurricane vortex. They decrease rapidly to less than 5 m s^{-1} at the onset of RI, and achieve nearly a calm condition at the peak intensity stage, especially in the upper peak warming-core/outflow layer. The storm-relative flows become large again as Wilma weakens rapidly after an eyewall replacement cycle (ERC) [see *Chen et al.*, 2011]. The increased storm-relative flows coincide with the weakening of upper outflows as a result of forming a large outer eyewall after the ERC. The above results indicate the importance of storm-relative flows and VWS in the upper troposphere in determining the RI of Wilma.

[9] The second feature of relevance is the presence of a weak radial inflow layer of about 2–3 m s^{-1} above the upper-level outflow layer. In the quasi-balanced framework, this storm-scale inflow layer, which resides in the lower stratosphere, may be considered as being caused through mass continuity by the upper-level convergence and subsidence in the eye, based on the study of *Zhang and Kieu* [2006, see Figure 3 therein]. Note that a similar radial inflow layer has also appeared in previous modeling studies [e.g., *Rotunno and Emanuel*, 1987; *Liu et al.*, 1999] and even in a hurricane-like vortex in a dry atmosphere [*Mrowiec et al.*, 2011]. However, in those studies, it develops in the upper troposphere, rather than in the lower stratosphere, and generates a warm core at relatively lower altitudes. Nevertheless, we have seen little discussion in the literature on the relationship between the upper-level inflow, mass sink in the eye, warm core and outflow layers and surface pressure changes.

[10] For the above reason, Figure 3 shows the distribution of horizontal perturbation wind vectors in the upper inflow layer (i.e., at z = 17.5 km), i.e., after removing a subdomain-averaged east-southeasterly flow of 6 m s^{-1}. In contrast to divergent outflows in the layers below, the perturbation winds show a cyclonic inflow with weak winds in the (lower pressure) core region (roughly within a radius of 30 km from the eye center), although they are influenced by propagating gravity waves [*Liu et al.*, 1999]. Associated with the cyclonic inflow component is the distribution of spirally banded cloud hydrometeors, in the form of cloud ice and snow. The

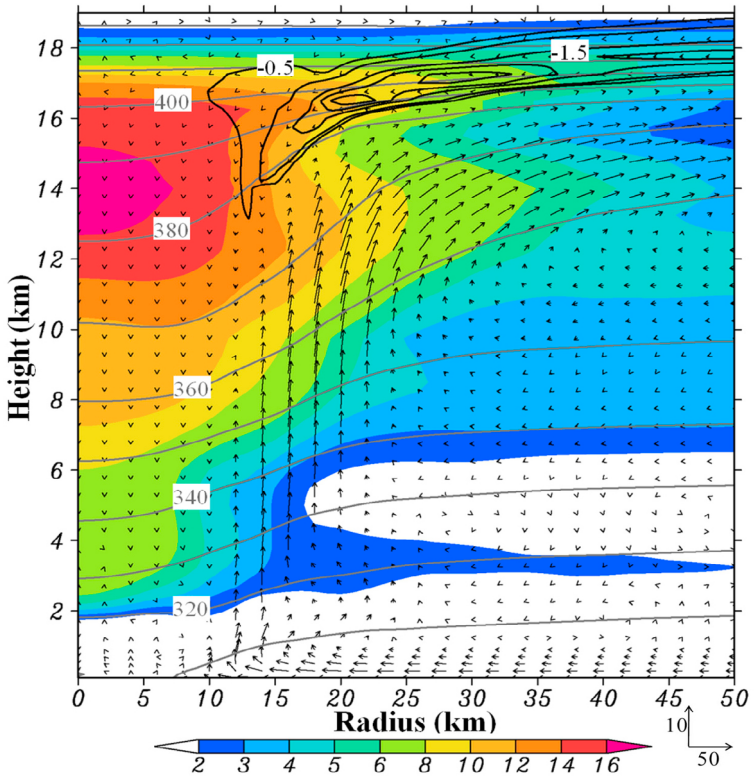

Figure 2. Radius-height cross section of temperature deviations (shaded) with respect to the (1000 km × 1000 km) area-averaged temperatures at the model initial time, superposed with potential temperature (θ, contoured at intervals of 10 K), in-plane flow vectors (see the speed scales at the bottom right, m s^{-1}), and the upper-level radial inflows (contoured at 0.5 m s^{-1}) from the 30-h prediction of Hurricane Wilma (2005).

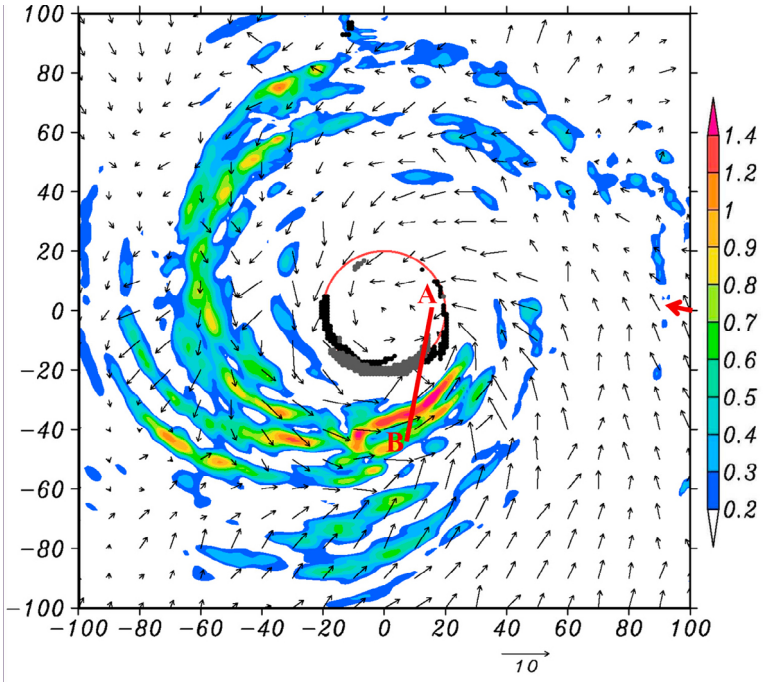

Figure 3. Distribution of cloud (ice and snow) hydrometeors (shaded, 10^{-3} g kg^{-1}), superposed with perturbation horizontal wind vectors, i.e., after removing the subdomain-averaged mean flow of 6 m s^{-1} (denoted by a red arrow) at z =17.5 km over a subdomain of 200 km × 200 km from the 30-h prediction. A red circle denotes the radius of maximum wind (RMW) at z = 11 km, and black and grey dots near the RMW indicate the distribution of convective bursts at 30 h, and 30 h 5 min, respectively. Line AB denotes the location of vertical cross section used in Figure 4.

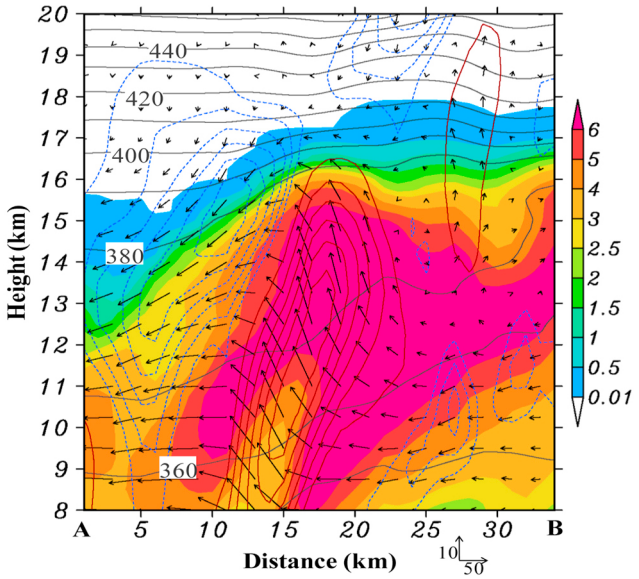

Figure 4. Vertical cross section of cloud (ice, snow and graupel) hydrometeors (shaded, g kg^{-1}), superposed with in-plane storm-relative flow vectors (see the speed scales at the bottom right, m s^{-1}) and vertical motion (downward motion by dashed lines in blue at intervals of 1 m s^{-1} and upward motion by solid lines in red at intervals of 3 m s^{-1}) along line AB given in Figure 3. The null vertical motion contour is omitted.

minimum temperature in the cloudy region at this level is 197 K, which is clearly in a stratospheric layer. These stratospheric cloud hydrometeors must be produced by overshooting CBs, which are defined herein as ~~meso-beta-scale~~ convective systems consisting of updrafts of at least 15 m s^{-1} in the upper troposphere (i.e., above z = 11 km). *Houze et al.* [2009] also analyzed such deep, intense convective updrafts in Hurricane Ophelia (2005) from Doppler radar data. One can see that the CBs, taken at the two times at a 5-minute interval, develop in the vicinity of the radius of maximum wind (RMW), where the highest equivalent potential temperature in the eyewall is typically present [see *Liu et al.*, 1999, Figure 3 therein]. These CBs decrease in intensity as they overshoot slantwise outward into the lower stratosphere, leaving their footprints as the spiral cloud bands aloft. Thus, the more pronounced converging inflows within the inner-core region enclosed by spiral cloud bands are indicative of the collective mass detrainment into the eye from the CBs (and deep convection in general) in the eyewall. It is this horizontal convergence or inflow that is closely related to the eye subsidence accounting for the formation of a warm core within the upper outflow layer (cf. Figures 2 and 3).

[11] The vertical circulation characteristics of a single CB are given in Figure 4, which shows a deep layer of an intense updraft with a radial width of about 10 km (also see Figure 3), and a peak magnitude of more than 18 m s^{-1} near z = 11 km; its cloud top reaches an altitude of about 18 km. Typically, it has an azimuthal scale of several tens of kilometers (Figure 3). The life time of the CB, traced at z = 11 km from its initiation to dissipation at a nearly vanishing intensity, is about 30 minutes (not shown). Of particular interest is that the CB-induced compensating subsidence, characterized by its peak amplitude of more than 5 m s^{-1} and a depth of more than 10 km, is mostly inward, accounting for the downward tilt of isentropic surfaces in the core region. Such strong subsidence has been observed in Hurricane Bonnie (1998) by *Heymsfield et al.* [2001]. More intense subsidence occurs in the cloud region, suggesting the possible enhanced effects of sublimative cooling of cloud hydrometeors and (long-wave) radiation-cloud interaction, as shown by *Liu et al.* [1999]; this can also be seen from the general converging flows in the vicinity of the spiral cloud bands. Nevertheless, the CB-induced subsidence in the cloud-free region can be as strong as 2–3 m s^{-1} and extend to z = 19 km. Note that this subsidence tends to propagate cyclonically downstream in the eye, as shown by *Liu et al.* [1999]. This is why the vertical cross section used in Figure 4 is not radially taken. Note also that the CBs occur mostly on the upshear quadrant of the eyewall, even though the VWS is weak (cf. Figures 3 and 1, top); these CBs propagate cyclonically in the eyewall at the rates slower with the mean flow. This is consistent with the observational findings of *Reasor et al.* [2009] for Hurricane Guillermo (1997).

4. Concluding Remarks

[12] In this study, CBs, the upper-level warm core and flow structures in relation to the RI of a tropical cyclone are examined using a 72-h nested-grid, cloud-permitting prediction of Hurricane Wilma (2005). Results show the formation of an upper-level warming core, coinciding with the onset of RI, due to the descent of stratospheric air. An isentropic analysis reveals more than 7-km descent of the stratospheric air, causing a warming core of more than 18°C in the eye that is located in the same layer as the upper outflow during the RI stage. It is found that the warm core in the eye results from the detrainment of CBs that occur mostly in the vicinity of the RMW where higher equivalent potential temperature is located. Then, the CBs' detrainment enhances collectively cyclonic radial inflows above the upper-level outflow layer that are associated with the mass sink in the eye, leading to the subsidence warming below with the peak intensity occurring in the same layer as the upper-level outflow. This finding confirms our hypothesis that a strong divergent outflow in the outer region helps protect the warm core from ventilation by environmental flows. Based on a hydrostatic argument, we conclude that the upper-level warming in the eye, especially with stratospheric origin, is more effective than the lower-level warming in causing surface pressure falls, and recommend that more attention be paid to the magnitude of storm-relative flows and VWS in the upper troposphere, rather than just VWS in the typical 850–200 hPa layer, in order to reasonably predict the RI of tropical cyclones.

[13] In a forthcoming journal article, we will show that the development of CBs, the intensity and evolution of the upper-level warming core as well as the RI of Wilma, depend critically on the magnitude of SSTs and the vertical resolution of the WRF model. RI of the boundary-layer rotational flows in relation to rapid drops in P_{MIN} and contraction of the RMW will also be explored. Furthermore, more RI case studies need to be conducted to examine the validity of the above-mentioned hypothesis.

[14] **Acknowledgments.** The model integration was completed on NOAA's NJET supercomputer through the Hurricane Forecast Improvement Program. This work was supported by NASA grant 1284085, ONR grant N000140710186, and NSF ATM0758609.

References

Barnes, G. M., and P. Fuentes (2010), Eye excess energy and the rapid intensification of Hurricane Lili (2002), *Mon. Weather Rev.*, *138*, 1446–1458, doi:10.1175/2009MWR3145.1.

Black, M. L., J. F. Gamache, F. D. Marks Jr., C. E. Samsury, and H. E. Willoughby (2002), Eastern Pacific Hurricanes Jimena of 1991 and Olivia of 1994: The effect of vertical shear on structure and intensity, *Mon. Weather Rev.*, *130*, 2291–2312, doi:10.1175/1520-0493(2002)130<2291:EPHJOA>2.0.CO;2.

Bosart, L. F., W. E. Bracken, J. Molinari, C. S. Velden, and P. G. Black (2000), Environmental influences on the rapid intensification of Hurricane Opal (1995) over the Gulf of Mexico, *Mon. Weather Rev.*, *128*, 322–352, doi:10.1175/1520-0493(2000)128<0322:EIOTRI>2.0.CO;2.

Braun, S. A., and L. Wu (2007), A numerical study of Hurricane Erin (2001). Part II: Shear and the organization of eyewall vertical motion, *Mon. Weather Rev.*, *135*, 1179–1194, doi:10.1175/MWR3336.1.

Braun, S. A., M. T. Montgomery, and Z. Pu (2006), High-resolution simulation of Hurricane Bonnie (1998). Part I: The organization of eyewall vertical motion, *J. Atmos. Sci.*, *63*, 19–42, doi:10.1175/JAS3598.1.

Chen, H., D.-L. Zhang, J. Carton, and R. Atlas (2011), On the rapid intensification of Hurricane Wilma (2005). Part I: Model prediction and structural changes, *Weather Forecast.*, *26*, 885–901, doi:10.1175/WAF-D-11-00001.1.

Eastin, M. D., W. M. Gray, and P. G. Black (2005), Buoyancy of convective vertical motions in the inner core of intense hurricanes. Part II: Case studies, *Mon. Weather Rev.*, *133*, 209–227, doi:10.1175/MWR-2849.1.

Fierro, A. O., and J. M. Reisner (2011), High-resolution simulation of the electrification and lightning of Hurricane Rita during the period of rapid intensification, *J. Atmos. Sci.*, *68*, 477–494, doi:10.1175/2010JAS3659.1.

Frank, W. M., and E. A. Ritchie (2001), Effects of vertical wind shear on the intensity and structure of numerically simulated hurricanes, *Mon. Weather Rev.*, *129*, 2249–2269, doi:10.1175/1520-0493(2001)129<2249:EOVWSO>2.0.CO;2.

Halverson, J. B., J. Simpson, G. Heymsfield, H. Pierce, T. Hock, and E. A. Ritchie (2006), Warm core structure of Hurricane Erin diagnosed from high altitude dropsondes during CAMEX-4, *J. Atmos. Sci.*, *63*, 309–324, doi:10.1175/JAS3596.1.

Hawkins, H. F., and S. M. Imbembo (1976), The structure of a small, intense hurricane—Inez 1966, *Mon. Weather Rev.*, *104*, 418–442, doi:10.1175/1520-0493(1976)104<0418:TSOASI>2.0.CO;2.

Hawkins, H. F., and D. T. Rubsam (1968), Hurricane Hilda, 1964. II: Structure and budgets of the hurricane core on October 1, 1964, *Mon. Weather Rev.*, *96*, 617–636, doi:10.1175/1520-0493(1968)096<0617:HH>2.0.CO;2.

Heymsfield, G. M., J. B. Halverson, J. Simpson, L. Tian, and T. P. Bui (2001), ER-2 Doppler radar investigations of the eyewall of Hurricane Bonnie during the Convection and Moisture Experiment-3, *J. Appl. Meteorol.*, *40*, 1310–1330, doi:10.1175/1520-0450(2001)040<1310:EDRIOT>2.0.CO;2.

Hirschberg, P. A., and J. M. Fritsch (1993), On understanding height tendency, *Mon. Weather Rev.*, *121*, 2646–2661, doi:10.1175/1520-0493(1993)121<2646:OUHT>2.0.CO;2.

Holland, G. J. (1997), The maximum potential intensity of tropical cyclones, *J. Atmos. Sci.*, *54*, 2519–2541, doi:10.1175/1520-0469(1997)054<2519:TMPIOT>2.0.CO;2.

Holliday, C. R., and A. H. Thompson (1979), Climatological characteristics of rapidly intensifying typhoons, *Mon. Weather Rev.*, *107*, 1022–1034, doi:10.1175/1520-0493(1979)107<1022:CCORIT>2.0.CO;2.

Hong, X. D., S. W. Chang, S. Raman, L. K. Shay, and R. Hodur (2000), The interaction between Hurricane Opal (1995) and a warm core ring in the Gulf of Mexico, *Mon. Weather Rev.*, *128*, 1347–1365, doi:10.1175/1520-0493(2000)128<1347:TIBHOA>2.0.CO;2.

Houze, R. A., Jr., W.-C. Lee, and M. M. Bell (2009), Convective contribution to the genesis of Hurricane Ophelia (2005), *Mon. Weather Rev.*, *137*, 2778–2800, doi:10.1175/2009MWR2727.1.

Kaplan, J., and M. DeMaria (2003), Large-scale characteristics of rapidly intensifying tropical cyclones in the North Atlantic basin, *Weather Forecast.*, *18*, 1093–1108, doi:10.1175/1520-0434(2003)018<1093:LCORIT>2.0.CO;2.

Kaplan, J., M. DeMaria, and J. A. Knaff (2010), A revised tropical cyclone rapid intensification index for the Atlantic and eastern North Pacific Basins, *Weather Forecast.*, *25*, 220–241, doi:10.1175/2009WAF2222280.1.

Kossin, J. P., and M. D. Eastin (2001), Two distinct regimes in the kinematic and thermodynamic structure of the hurricane eye and eyewall, *J. Atmos. Sci.*, *58*, 1079–1090, doi:10.1175/1520-0469(2001)058<1079:TDRITK>2.0.CO;2.

LaSeur, N. E., and H. F. Hawkins (1963), An analysis of Hurricane Cleo (1958) based on data from research reconnaissance aircraft, *Mon. Weather Rev.*, *91*, 694–709, doi:10.1175/1520-0493(1963)091<0694:AAOHCB>2.3.CO;2.

Liu, Y., D.-L. Zhang, and M. K. Yau (1997), A multiscale numerical study of Hurricane Andrew (1992). Part I: Explicit simulation and verification, *Mon. Weather Rev.*, *125*, 3073–3093, doi:10.1175/1520-0493(1997)125<3073:AMNSOH>2.0.CO;2.

Liu, Y., D.-L. Zhang, and M. K. Yau (1999), A multiscale numerical study of Hurricane Andrew (1992). Part II: Kinematics and inner-core structures, *Mon. Weather Rev.*, *127*, 2597–2616, doi:10.1175/1520-0493(1999)127<2597:AMNSOH>2.0.CO;2.

Malkus, J. S., and H. Riehl (1960), On the dynamics and energy transformations in steady-state hurricanes, *Tellus*, *12*, 1–20, doi:10.1111/j.2153-3490.1960.tb01279.x.

Molinari, J., P. K. Moore, V. P. Idone, R. W. Henderson, and A. B. Saljoughy (1994), Cloud-to-ground lightning in Hurricane Andrew, *J. Geophys. Res.*, *99*, 16,665–16,676, doi:10.1029/94JD00722.

Molinari, J., P. K. Moore, and V. P. Idone (1999), Convective structure of hurricanes as revealed by lightning locations, *Mon. Weather Rev.*, *127*, 520–534, doi:10.1175/1520-0493(1999)127<0520:CSOHAR>2.0.CO;2.

Montgomery, M. T., M. M. Bell, S. D. Aberson, and M. L. Black (2006), Hurricane Isabel (2003): New insights into the physics of intense storms. Part I: Mean vortex structure and maximum intensity estimates, *Bull. Am. Meteorol. Soc.*, *87*, 1335–1347, doi:10.1175/BAMS-87-10-1335.

Mrowiec, A. A., S. T. Garner, and O. M. Pauluis (2011), Axisymmetric hurricane in a dry atmosphere: Theoretical framework and numerical experiments, *J. Atmos. Sci.*, *68*, 1607–1619, doi:10.1175/2011JAS3639.1.

Price, C., M. Asfur, and Y. Yair (2009), Maximum hurricane intensity preceded by increase in lightning frequency, *Nat. Geosci.*, *2*, 329–332, doi:10.1038/ngeo477.

Reasor, P. D., M. D. Eastin, and J. F. Gamache (2009), Rapidly intensifying Hurricane Guillermo (1997). Part I: Low-wavenumber structure and evolution, *Mon. Weather Rev.*, *137*, 603–631, doi:10.1175/2008MWR2487.1.

Rodgers, E. B., W. S. Olson, V. M. Karyampudi, and H. F. Pierce (1998), Satellite-derived latent heating distribution and environmental influences in Hurricane Opal (1995), *Mon. Weather Rev.*, *126*, 1229–1247, doi:10.1175/1520-0493(1998)126<1229:SDLHDA>2.0.CO;2.

Rogers, R. (2010), Convective-scale structure and evolution during a high-resolution simulation of tropical cyclone rapid intensification, *J. Atmos. Sci.*, *67*, 44–70, doi:10.1175/2009JAS3122.1.

Rotunno, R., and K. A. Emanuel (1987), An air–sea interaction theory for tropical cyclones. Part II: Evolutionary study using a nonhydrostatic axisymmetric numerical model, *J. Atmos. Sci.*, *44*, 542–561, doi:10.1175/1520-0469(1987)044<0542:AAITFT>2.0.CO;2.

Shay, L. K., G. J. Goni, and P. G. Black (2000), Effects of a warm oceanic feature on Hurricane Opal, *Mon. Weather Rev.*, *128*, 1366–1383, doi:10.1175/1520-0493(2000)128<1366:EOAWOF>2.0.CO;2.

Wang, Y., and G. J. Holland (1996), Tropical cyclone motion and evolution in vertical shear, *J. Atmos. Sci.*, *53*, 3313–3332, doi:10.1175/1520-0469(1996)053<3313:TCMAEI>2.0.CO;2.

Zhang, D.-L., and J. M. Fritsch (1988), Numerical sensitivity experiments of varying model physics on the structure, evolution and dynamics of two mesoscale convective systems, *J. Atmos. Sci.*, *45*, 261–293, doi:10.1175/1520-0469(1988)045<0261:NSEOVM>2.0.CO;2.

Zhang, D.-L., and C. Q. Kieu (2006), Potential vorticity diagnosis of a simulated hurricane Part II: Quasi-balanced contributions to forced secondary circulations, *J. Atmos. Sci.*, *63*, 2898–2914, doi:10.1175/JAS3790.1.

H. Chen and D.-L. Zhang, Department of Atmospheric and Oceanic Science, University of Maryland, College Park, MD 20742-2425, USA. (dalin@atmos.umd.edu)